Composites Part B 161 (2019) 617–626

Contents lists available at ScienceDirect

Composites Part B

journal homepage: www.elsevier.com/locate/compositesb

Layered hybrid composites using multi-walled carbon nanotube film as reflection layer and multi-walled carbon nanotubes/neodymium magnet/epoxy as absorption layer perform selective electromagnetic interference shielding

Ming-Yao Li, Shivam Gupta, Ching Chang, Nyan-Hwa Tai*

Department of Materials Science and Engineering, National Tsing Hua University, Hsinchu, 300, Taiwan, ROC

A B S T R A C T

This work develops a unique layered structural composite to prevent the device from internal electromagnetic (EM) waves' self-disturbance and external EM wave interference. The composite is composed of two layers, the inner layer is a hybrid composite, using MWCNTs and NdFeB powders as fillers and epoxy as matrix, which is designed as absorbent layer, and the outer is MWCNT-coated non-woven fabric, which is treated as reflection layer. The inner layer containing MWCNTs and magnetic powder of NdFeB can firstly absorb parts of EM waves generating from inside devices, and when the rest EM waves transmit through the inner layer and impinge to the outer layer, almost all of the waves will be reflected back. The reflected waves will go through the inner layer and be absorbed again. In the meanwhile, as the external EM waves impinge to the outer layer, they will be reflected immediately. The optimal combination of this study is able to achieve over 92% (−23.09 dB) absorption and leave least than 8% (−11 dB) reflection of internal EM waves, and over 99.99% reflection of external EM waves.

1. Introduction

With the rapid development of the electrical industry, electromagnetic interference (EMI) has become a serious problem in nowadays' society. Electronic devices such as mobile phone, laptops, radio etc. have become part of our life due to their significant advancement to our society, and make our daily life a lot more convenience. However, these electronic devices generate electromagnetic interference of radio frequency radiation, which adversely degrades the device and possibly cause the malfunction of it. Additionally, these radiations may cause harm to human beings [1]. Therefore, it is urgent to develop EMI shielding materials to reduce the EMI pollution.

Electromagnetic interference shielding effectiveness represents the ability of a material to block the undesired EM waves [2–4]. There are two important mechanisms in EMI shielding: reflection and absorption. Mostly, reflection is the most significant factor, and related to the interaction between the conducting parts of the material and the impinging electromagnetic field. While absorption is related to the absorption of EM waves by the materials that has high electric permittivity or high magnetic permeability. However, the self-reflected EM waves may possibly cause self-disturbance, so it is also critical to develop a material with high EM wave absorption efficiency.

Metal-based materials are widely used to protect devices from electromagnetic interference disturbance due to their high electrical conductivity and a high dielectric constant [5–7]. However, metal-based materials corrode easily and are quite heavy, which compromise their practical usage as EMI shielding material. Also, the metal-based materials tend to block the EM waves through reflection, which increases the possibility of self-disturbance to the device. Compared with conventional metal-based EMI shielding materials, conductive polymer composites have recently gained popularity because of their low cost, lightweight, resistant to corrosion, flexibility and easy processing [8–11]. To fabricate conductive polymer composites, conductive fillers are generally introduced to non-conductive matrix. Metallic fillers, carbonaceous fillers and conjugated polymers such as polyaniline have been incorporated into the polymer [12–14]. Epoxy, one of the most widely used thermosetting polymer, possesses all the aforementioned advantages for polymer, and is used in wide range of applications. Other polymers like polypropylene, polymethylmethacrylate and polyether sulfones as the matrixes for electromagnetic interference shielding materials have also been studied [2,15,16].

To form a long range conductive path within the matrix, the amount of the fillers must meet the percolation threshold [17,18]. Generally, fillers with higher aspect ratio and better dispersion properties have lower percolation threshold value [19]. Multi-walled carbon nanotubes (MWCNTs) have outstanding mechanical, electrical properties as well as their unique structure such as high aspect ratio and low density, which make them easier to create a conductive network for excellent

* Corresponding author.
E-mail address: nhtai@mx.nthu.edu.tw (N.-H. Tai).

https://doi.org/10.1016/j.compositesb.2018.12.130
Received 31 August 2018; Received in revised form 27 December 2018; Accepted 30 December 2018
Available online 02 January 2019
1359-8368/

performance in EMI shielding at relatively low loading [20,21]. Reports show that the EMI shielding efficiency was proportional to the concentration of MWCNTs in the polymer matrix, even if the electrical conductivities of the composites were identical due to the excessive MWCNTs content in the composites. It suggests that the MWCNTs not only enhance the electric networks, but also absorb EM waves in the composites [22,23].

In order to select proper materials for EMI absorption, high dielectric and coercive forces must be considered because electromagnetic waves are attenuated by the electric and magnetic fields of the shielding materials. The incoming EM waves can be absorbed and dissipated into heat through magnetic losses and dielectric losses. Studies show that with the presence of more metallic and magnetic materials in the composite, the absorbed EM waves are increase. Carbon materials decorated with silver and nickel nanoparticles have excellent EMI shielding efficiency with absorption dominated mechanism [12]. Published articles also show that MWCNTs containing Fe catalyst incorporated with PMMA as well as Fe encapsulated within MWCNTs have better absorption of EM waves than that of reflection [24,25]. Recently, hard ferrite with high coercivity as well as a huge energy product has been employed as one of the candidates for EM wave absorption material [26,27]. Neodymium magnet (NdFeB) is known as one of the strongest magnets that has high energy product and high coercivity, which make it a potential material for absorbing EM waves.

Layered structure composites to enhance EMI shielding effectiveness have been adopted in prior studies [28–31]. Layer-structured fabric-supported polyaniline/cobalt-nickel composites were reported with total EMI shielding effectiveness of 46.22 dB [29]. It was found that the layered structure performed better compared with their single peer. A binary blend of polycarbonate and polyvinylidene fluoride (PVDF) was also reported as a matrix for the fillers of manganese dioxide-doped MWCNTs and a three-dimensional cross-linked graphene oxide doped with ferrite nanoparticles [30]. When the composites were rationally stacked into a multilayer architecture, the EM waves followed an absorption-multiple reflection-absorption pathway and the EMI shielding significantly enhanced. Construction of layer-by-layer architectural assembly in which PVDF/MWCNTs/Mn−Fe nanoparticles as outer layer and PVDF/nickel-deposited woven carbon fiber as inner layer was also reported for the high absorption dominant EMI shielding effectiveness [31]. However, most of the layered composites were thick in thickness and the fabrication processes were complicate, which hindered their practical usages. In addition, most of the studies in layered composites focused on the enhancement of total EMI shielding effectiveness, and a few of them focused on improving the absorption of EM waves. Therefore, it is critical to develop a composite which possesses great EMI shielding effectiveness as well as great ability to absorb EM waves.

In this work, a unique and uncomplicated multilayer structure with high EMI shielding effect and absorption as the main shielding mechanism was designed. The structure is composed of two layers, the inner layer is MWCNTs/NdFeB/epoxy composite which is designed as absorbent layer, and the outer is MWCNT film which is treated as reflection layer, as shown in Fig. 1. The inner layer with MWCNTs and magnetic powder of NdFeB are targeting at absorbing EM waves. On the contrary, the outer MWCNT film will reflect almost all the EM waves away. This design makes sure that almost no EM wave penetrate out of the device and reduce the possibility of self-disturbance. Also, it successfully blocks the external EM waves. Such structure has easier process comparing with the conventional EMI shielding materials targeting at increasing absorption.

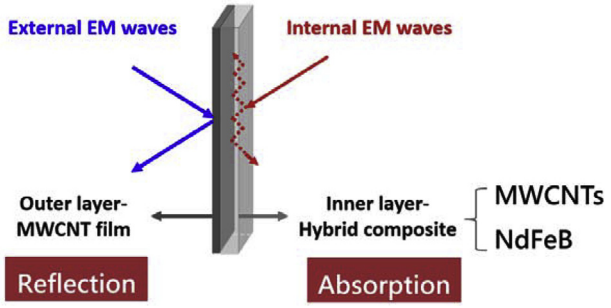

Fig. 1. Schematic figure of EMI shielding of the layered composites.

2. Experimental

2.1. Materials

The non-woven fabric (Grade3254, 81.1 g/m^2) was purchased from Ahlstrom-Munksjö and the composition is polyethylene terephthalate (PET). The waterborne dispersion of MWCNT used for MWCNT film as the outer layer was purchased from Taiwan Carbon Nano Technology Corporation (CDW-181). The percentage of MWCNTs in the dispersion is 3%, and the diameter and length are 10 nm and 1.5 μm, respectively. The MWCNT powders, used as fillers for the inner layer with diameter around 20–30 nm and length around 1 μm, were purchased from Golden Innovation Business Corporation. The unmagnetized Neodymium magnet powder was purchased from Taiwan Magnetic Corporation, and the diameter of the magnetic particles is 30–40 μm. The epoxy was purchased from Hsin-Han Corporation (epoxy resin: E-120C; hardener: H-100), and the weight ratio of resin to hardener is 3:1.

2.2. Preparation of MWCNT layer

The MWCNT film was coated on the non-woven fabric by cast knife with the height of 250 μm, as shown in Fig. 2a. After dry out the solvent on a hot plate at 120 °C for 1 h. For doing the above step once is defined as one layer of MWCNT film, and doing the above step for ten times is defined as ten layers of MWCNT film. This MWCNT film was treated as the outer layer of the hybrid composite.

2.3. Preparation of epoxy composite layer

The epoxy composite layer is treated as the inner layer of the hybrid composite. One, three, five and seven weight percent of MWCNTs; 10, 20, and 30 wt% of NdFeB powder along with epoxy were firstly mixed by a glass rod to prepare different composites, and the conversion between weight and volume fractions of the fabricated samples is given in Table 1. Superior connection as well as better electric conductivity of nano-fillers result in a better EMI shielding efficiency. The dispersion of MWCNTs is a critical issue, so here we introduce a three roll-milling machine shown in Fig. 3 (TR35W, Yeong-Shin, Taiwan), which applied a large shear force on the blender to improve the dispersion [32]. The pre-mixture of MWCNTs, NdFeB powders and epoxy was then passed through the machine for twenty times to achieve better dispersion. The gap between two parallel rollers was tunable and the smallest gap was 20 μm, and rotation speed was fixed at 150 rpm. The mixture was collected from the removal knife and poured into a rectangular mold of 2.5 × 2.5 cm^2 x 1 mm placed on the MWCNT film as shown in Fig. 2b and c. The whole sample was further hot pressed at 70 °C for 1 h and 120 °C for 4 h to cure the epoxy, as depicted in Fig. 2d.

2.4. Material characterizations

In this work, the structure and the composition of the non-woven fabric, MWCNT film, unmagnetized NdFeB and NdFeB/MWCNTs/

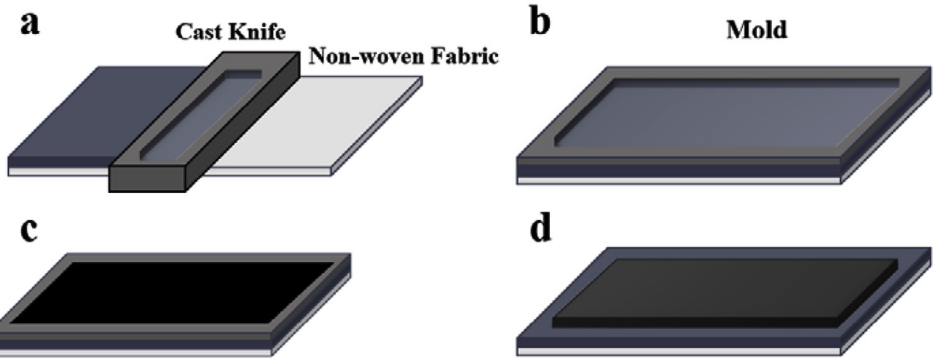

Fig. 2. Schematic figures of the fabrication process. (a) MWCNT film casting by cast knife; (b) rectangular mold was placed on the casted film; (c) pour the post-mixture into the mold; (d) hot-pressed the composite film.

Table 1
Ratios of MWCNT and NdFeB and conversion between weight and volume fractions of the fabricated samples.

Weight Ratio	Volume Ratio
1 wt.% MWCNT/10 wt.% NdFeB	0.58 vol% MWCNT/1.61 vol% NdFeB
5 wt.% MWCNT/10 wt.% NdFeB	2.94 vol% MWCNT/1.65 vol% NdFeB
7 wt.% MWCNT/10 wt.% NdFeB	4.16 vol% MWCNT/1.66 vol% NdFeB
5 wt.% MWCNT/10 wt.% NdFeB	2.94 vol% MWCNT/1.65 vol% NdFeB
5 wt.% MWCNT/20 wt.% NdFeB	3.25 vol% MWCNT/3.64 vol% NdFeB
5 wt.% MWCNT/30 wt.% NdFeB	3.64 vol% MWCNT/3.11 vol% NdFeB

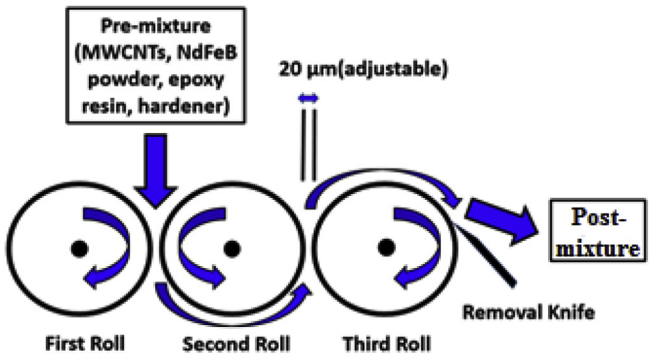

Fig. 3. Schematic of a three roll-milling process.

Epoxy composite were characterized using X-ray diffraction (XRD, Shimadzu XRD600). Raman spectrometry (Raman-LabRam HR800) equipped with a He−Ne laser beam with a wavelength of 632.8 nm were employed to characterize the difference between the waterborne dispersion MWCNTs and the conventional MWCNT powders. The magnetic property of the designed composite was obtained by superconducting quantum interference device (SQUID) at room temperature (300 K). The morphologies and the microstructure of MWCNT film and NdFeB/MWCNTs/Epoxy composites were studied using a field emission scanning electron microscope (FESEM, JEOL 6500F). A four-probe electric measuring instrument (CT5601Y, Chitai Electronic Corp.) was employed for the measurement of electrical conductivity.

2.5. EMI shielding efficiency measurement

The EMI shielding efficiencies were measured through a network analyzer (Alight Technologies, E8364A, PNA series Network Analyzer), and the network analyzer was connected with a rectangular waveguide (WR-90). The tests were performed at frequencies of X band, ranging from 8.2 GHz to 12.4 GHz. The specimen with a cross-sectional area of $2.50 \times 2.50\ cm^2$ was placed between the two sections of the waveguide, and the dimension of the waveguide is $2.30 \times 1.00\ cm^2$. The S-parameters (S_{11}, S_{12}, S_{22}, S_{21}) of each sample were recorded to obtain both transmission loss and reflection loss. To study the permittivity and permeability of the absorbent layer, the samples were fabricated into hollow cylindrical shape with dimensions of 3.50, 3.04, and 10.0 mm for outer diameter, inner diameter, and length, respectively. To fabricate such sample, we poured the post-mixture into a Teflon cylindrical mold with the diameter of 3.50 mm, and placed a Teflon stick with the diameter of 3.04 in the center followed by a curing process at 120 °C for 4 h. The complex dielectric permittivity and complex magnetic permeability were measured via Transmission Reflection Line method with Agilient 85071E Materials Measurement Software. To investigate the influences on both permittivity and permeability with the addition of NdFeB magnetic powder in the layer along with MWCNTs, two samples were fabricated in the hollow cylindrical shape: one with 5 wt.% of MWCNTs and the other with 30 wt.% of NdFeB magnetic powders.

3. Results and discussion

3.1. Characterizations

To characterize the differences between the MWCNT powder and MWCNT film, the Raman scattering was employed. Raman scattering is sensitive to the electronic structure and is essential to characterize carbonaceous materials. Raman shift for both samples show D-band at around 1346 cm^{-1}, which relates to the disorder-induced phonon mode due to finite size crystals and defects; G band at around 1577 cm^{-1} is corresponding to the E_{2g} tangential stretching mode of an ordered graphitic structure with sp^2 hybridization [33]. The I_D/I_G ratio has been used to correlate the structural purity of graphitic materials. The Raman shift shown in Fig. 4a reveals that the I_D/I_G ratio of the MWCNT powders (curve i) in the absorbent layer is 1.485, and the I_D/I_G ratio of MWCNT film (curve ii) derived from the waterborne dispersion is 1.83. The higher I_D/I_G ratio indicates that the MWCNTs from waterborne dispersion possessed more defects and functional groups, which makes it disperse better in the solution. The 2D-band between 2680 and 2730 cm^{-1}, which is the first overtone of the D mode, provides the information about the degree of crystallinity of the MWCNTs. From Fig. 4a, it is clear that the MWCNTs derived from waterborne dispersion has poorer crystallinity. The well-dispersed MWCNTs in the solution makes it much easier to coat a smooth MWCNT film on the non-woven fabric.

Fig. 4b shows the magnetic hysteresis loop of the 5 wt.%MWCNT/30 wt.% NdFeB/Epoxy composites that obtained from SQUID. The composites show hard ferromagnetic property. The M_s value can be derived from the M versus 1/H curve when H goes to infinity, while the coercive field (Hc) and the remanent magnetization (M_r) values can be directly obtained from the hysteresis loop. From the figure we can see that the composite possesses a typical hard ferromagnetic property. It has high saturation magnetization (M_s) of 40.36 emu/g. The higher

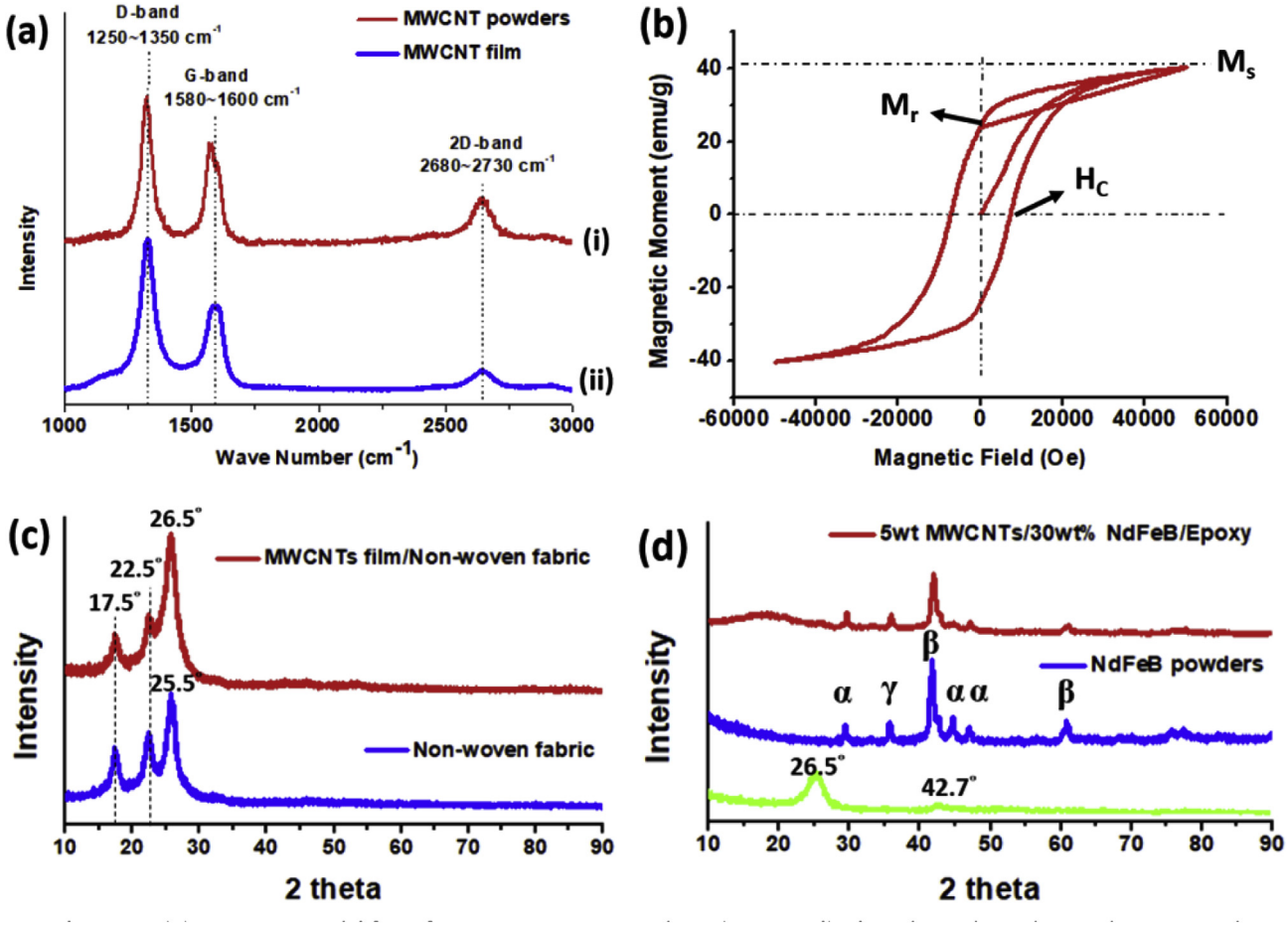

Fig. 4. (a) Raman shift of MWCNT powder (curve i) in the absorbent layer and MWCNT film (curve ii) in the reflection layer; (b) the magnetic hysteresis loop of the 5 wt.%MWCNT/30 wt.% NdFeB/Epoxy composite; (c) characterizations of non-woven fabric and MWCNT/non-woven fabric film using XRD; (d) characterizations of raw MWCNTs, raw NdFeB and 5 wt.% MWCNTs/30 wt.% NdFeB/Epoxy composite using XRD. Note that XRD patterns of mixed phases of NdFeB nanoparticles contain: $NdFeO_3$ (α), Fe_3O_4 (β) and B_2O_3 (γ).

saturation magnetization implies higher permeability, which benefits the absorption of EM waves. The composite also possesses high coercivity (Hc) at around 7500 Oe, which also contributes to the absorption of EM waves [34,35].

Fig. 4c shows the XRD pattern of the non-woven fabric and MWCNTs/Non-woven fabric hybrid film. The material of the non-woven fabric is PET. We can observe peaks at *2θ* around 17.5°, 22.5° and 25.5°, represent reflection characteristics of crystallinity relative to the planes (010), (110) and (100), respectively. The peaks of PET reveal that it has a semi-crystalline structure [36]. After coating MWCNT film on the PET substrate, we can observe that the peak shift slightly to 26.5°, which is the typical peak of MWCNTs. Fig. 4d shows the XRD pattern of MWCNTs, NdFeB powders and 5 wt%MWCNTs/30 wt% NdFeB/Epoxy composite. It can be seen that the XRD pattern of raw MWCNTs exhibits the typical peaks at *2θ* around 26.5° and 42.7°, corresponding to the normal structure of graphite (002) and (100) reflections (JCPDS No. 01–0646), respectively [37]. The XRD pattern of NdFeB revealed that it exhibits mixed phases including Fe_3O_4, $NdFeO_3$ (JCPDS No. 74–1473) and B_2O_3 [38,39]. These various oxide phases were also reported to possess a high dielectric constant, which leads to the increment in dielectric loss [40,41].

3.2. Morphologies

The side view morphologies of 1 layer and 10 layers of MWCNT films are shown in Fig. 5a and b, respectively. The MWCNTs are tightly coated on the non-woven fabric, and the surface seems very smooth and uniform. The thickness of one-layer film is around 11.8 μm, and 108.4 μm for 10 layers, which suggests that there is a superposition property between coating times and film thickness. The thickness of non-woven fabric is around 60 μm. The top view morphology of MWCNT film is shown in Fig. 5c. We can see that the MWCNTs are very dense and uniform on the non-woven fabric, thus create a very conductive film that is in favor of the reflection mechanism. Fig. 5d is the top view morphology of 5 wt%MWCNTs/30 wt%NdFeB epoxy composite. We can observe that the NdFeB nanoparticles and MWCNTs are uniformly dispersed in the epoxy matrix, and the diameter of the NdFeB particle is around 10 μm.

3.3. Electrical properties

The electrical resistivities (volume resistivity) of the composites were measured using the KeithLink resistivity apparatus Model LRS4-TG, equipped with a four-point probe. The four-point probe apparatus has four probes arranged in a straight line with equal spacing (s = 1.00 mm). The radius of the probe needle is 100 μm. A constant current (I) was supplied to pass through the two outer probes, and an output voltage (V) was measured across the inner probes using a voltmeter. The sheet resistivity can be calculated according to Ohm's Law: R_s = C.F.* (V/I), where C.F. is a correction factor. We can further derive the volume resistivity by the equation: $\rho_v = R_s * t$, where t is the thickness of the sample.

The volume resistivity of the MWCNT film and different composition of the hybrid composites are shown in Fig. 6. We can see that with

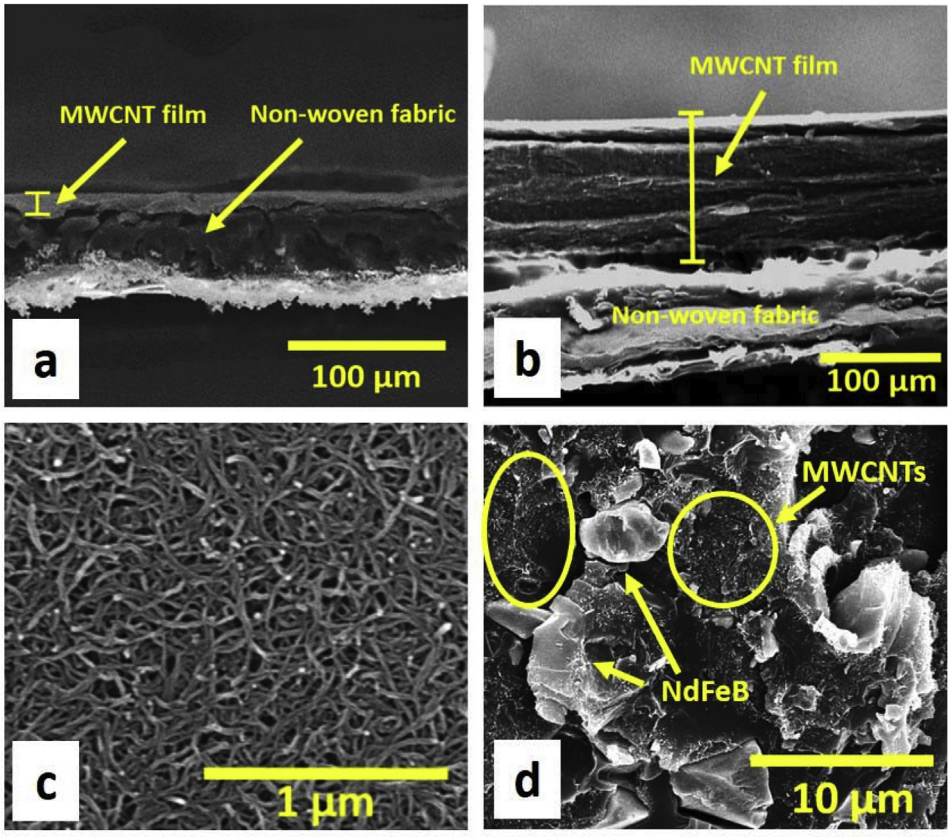

Fig. 5. SEM images of (a, b) Side-view of 1 layer and 10 layers of MWCNTs on non-woven fabric; (c) top-view of MWCNTs on non-woven fabric; (d) top-view of 5 wt.% MWCNTs/30 wt.% NdFeB/Epoxy composite.

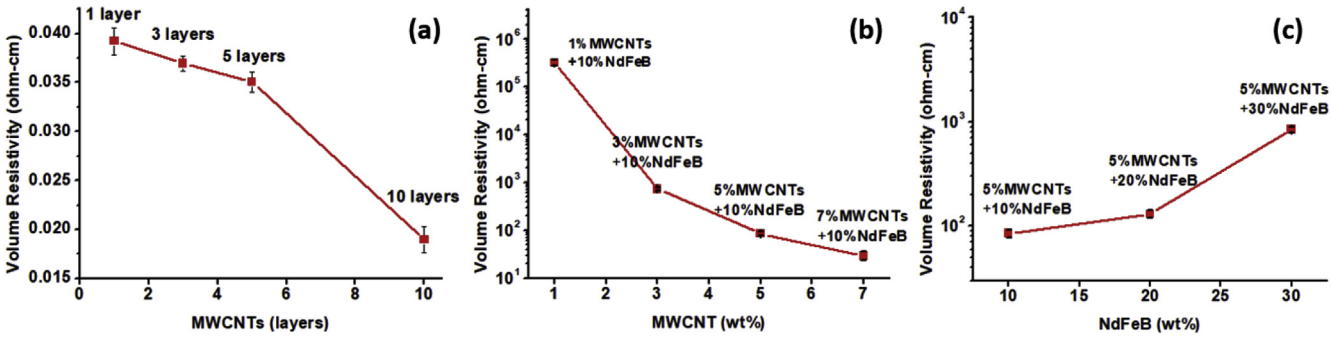

Fig. 6. Volume resistivity of (a) Different layer number of MWCNT film; (b) different concentration of MWCNTs with fixed concentration of NdFeB magnet; (c) different concentration of NdFeB magnet with fixed concentration of MWCNTs.

the increase of the MWCNT layer number, the volume resistivity decreases, as shown in Fig. 6a, which implies that there exists a positive correlation between the electrical conductivity and the extent of intercalations of MWCNTs. The reduction in volume resistivity causes the increment in electric conductivity, which enlarges the impedance mismatch, and therefore increases the reflection. Fig. 6b shows the volume resistivities of different concentrations of MWCNTs with the fixed concentration of NdFeB in the hybrid composite. With the increase of the MWCNTs, the volume resistivities decreases drastically from 10^{-5} to $10^{-3}\,\Omega$/sq. Thus, it suggests that MWCNTs play an important role in building the conductive path within the epoxy composite. Fig. 6c shows the volume resistivities of different concentrations of NdFeB with the fixed concentration of MWCNTs. It is obvious that the electrical conductivity decreases slightly with the increase of NdFeB in the hybrid composite owing to the mixed oxide phases of the NdFeB, which benefits the reduction in impedance mismatch as well as the reduction in reflection. According to the results, we can conclude that the amount of MWCNTs inside the hybrid composites is the dominant factor for the electrical conductivity.

3.4. Performance of EMI shielding efficiency

When the EM waves impinge on the material, the total EMI shielding efficiency (SE_{Total}) is contributed by reflection, absorption and multi-reflection, which can be expressed by Eq. (1) listed as follows:

$$SE_{Total}\,(dB) = SE_R + SE_A + SE_M \quad (1)$$

where SE_R, SE_A and SE_M represent the shielding efficiency due to reflection, absorption and multi-reflection, respectively. The SE_R and SE_A terms can be expressed by Eq. (2) and Eq. (3) [42]. SE_M is negligible when SE_A is higher than 10 dB because SE_M is a correction term [21].

$$SE_R = 10\log(1 - R) \quad (2)$$

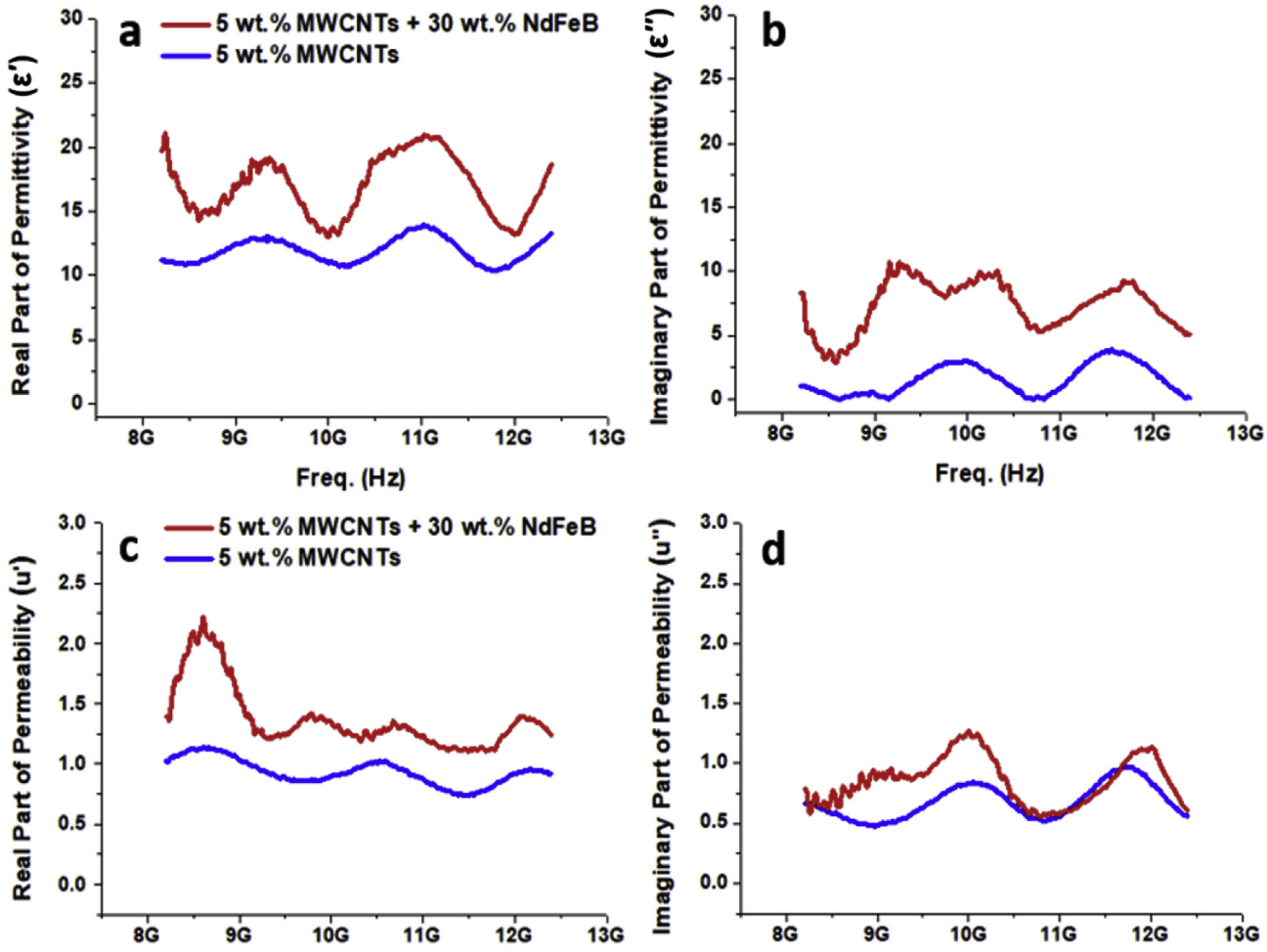

Fig. 7. Plots of (a) Real part of dielectric permittivity ε′; (b) imaginary part of dielectric permittivity ε″; (c) real part of magnetic permeability μ′; (d) imaginary part of magnetic permeability μ″.

Table 2
Comparison of permittivity and permeability between the composites fabricated in this work and barium ferrite [26,46,47].

	ε‘	ε‘’	μ‘	μ‘’	Ref.
5%MWCNT/30%NdFeB/epoxy	17.0 ± 2.3	7.4 ± 1.9	1.38 ± 0.27	0.86 ± 0.19	This work
Barium ferrite@rGO	20.0 ± 2.5	12.5 ± 2.0	0.45 ± 0.08	0.1 ± 0.08	[23]
Barium ferrite@rEGO	2.4	0.1	1.0	0.7	[40]
Barium ferrite@wax	6.0 ± 1.2	2.8 ± 0.8	1.65 ± 0.05	–	[39]

$$SE_A = 8.87\gamma d \tag{3}$$

where R is reflection coefficient, which is defined by Eq. (4), γ is the propagation constant in the conducting medium, which can be expressed by Eq. (5), and d represents the thickness of the shielding material.

$$R = \left(\frac{Z_0 - Z_{in}}{Z_0 + Z_{in}}\right)^2 \tag{5}$$

$$\gamma = \omega\sqrt{\frac{\varepsilon'\mu}{2}}\left[\sqrt{\left(1 + \frac{(\sigma + \omega\varepsilon'')}{\omega\varepsilon'}\right)^2} + 1\right]^{1/2} \quad \omega = 2\pi f \tag{4}$$

where Z_0 is the characteristic impendence of free space defined as $Z_0 = \sqrt{\mu_0/\varepsilon_0}$, which is approximately equal to 377 Ω, and Z_{in} is the input impendence defined by Eq. (6), ε_0 and μ_0 in Eq. (5) are electrical permittivity and magnetic permeability in free space, respectively, and σ represents the electrical conductivity, f the frequency.

$$Z_{in} = Z'\frac{Z_0\cosh(\gamma d) + z'\sinh(\gamma d)}{z'\cosh(\gamma d) + Z_0\sinh(\gamma d)} \tag{6}$$

where Z′ is wave impedance, as expressed in Eq. (7):

$$Z' = \frac{|E|}{|H|} = \sqrt{\frac{j\omega\mu}{\sigma + j\omega\varepsilon}} \tag{7}$$

The total EMI shielding effectiveness is also defined as the ratio of the incident and transmitted energies of the EM waves:

$$SE_{Total} = 10\log\left(\frac{P_{in}}{P_{out}}\right) = 20\log\left(\frac{E_{in}}{E_{out}}\right) = 20\log\left(\frac{H_{in}}{H_{out}}\right)(dB) \tag{8}$$

where P_{in} and P_{out} are the powers of the incident and transmitted waves, respectively. The EMI shielding effectiveness is measured by the reduction of the incident power of the EM waves.

Reflection of the EM waves occurs mostly in the conducting materials. As EM waves impinge on the surface of the material, the free electrons on the surface of the material will begin to generate anti-

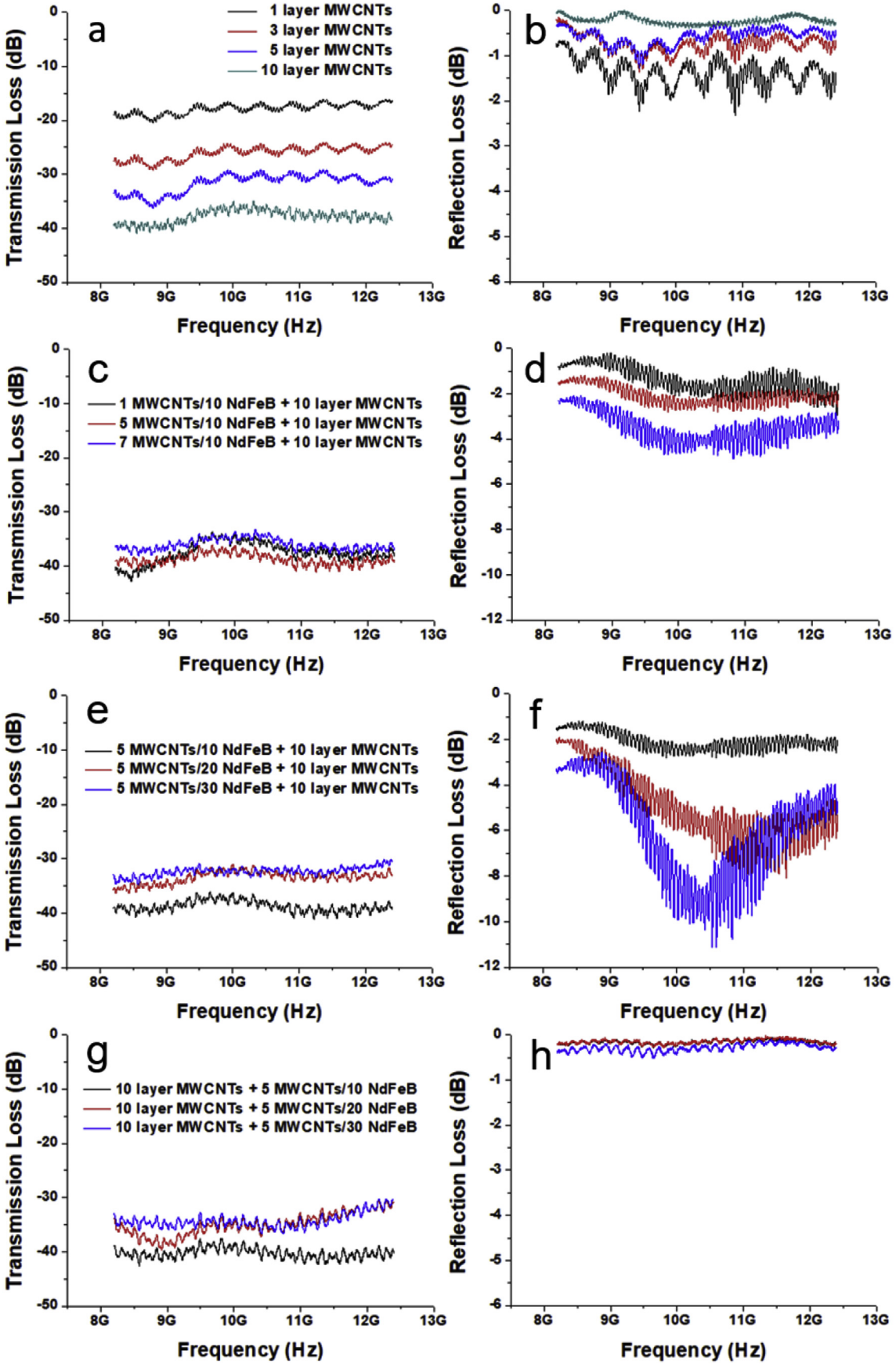

Fig. 8. Plots of EMI shielding effectiveness. (a, b) MWCNT films casted on non-woven fabric; (c, d) internal EM waves impinge on the samples possess same amount of NdFeB while changing MWCNT concentration; (e, f) internal EM waves impinge on the samples possess same amount of MWCNTs while changing NdFeB; (g, h) external EM waves impinge on the samples possess same amount of MWCNTs while changing NdFeB.

Table 3
The percentages of transmittance, reflection and absorption of the samples with different concentrations of MWCNTs and NdFeB magnet.

Samples		Transmission (loss in dB)	Reflection (loss in dB)	Absorption (loss in dB)
With 10 wt.% NdFeB	1 wt.% MWCNTs	0.006% (−42.22 dB)	79.432% (−1 dB)	20.562% (−41.22 dB)
	5 wt.% MWCNTs	0.010% (−40 dB)	63.095% (−2 dB)	36.895% (−38 dB)
	7 wt.% MWCNTs	0.025% (−36.02 dB)	39.810% (−4 dB)	60.165% (−32.02 dB)
With 5 wt.% MWCNTs	10 wt.% NdFeB	0.010% (−40 dB)	63.095% (−2 dB)	36.895% (−38 dB)
	20 wt.% NdFeB	0.032% (−34.94 dB)	19.953% (−7 dB)	80.015% (−27.94 dB)
	30 wt.% NdFeB	0.039% (−34.09 dB)	7.943% (−11 dB)	92.018% (−23.09 dB)

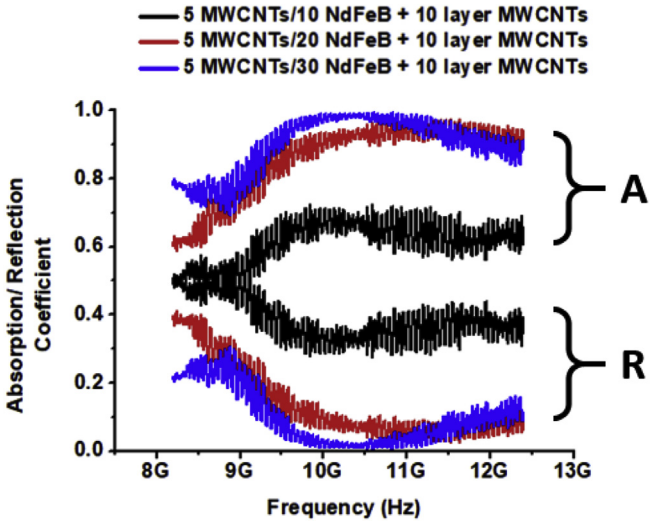

Fig. 9. The absorption coefficient (A) and reflection coefficient (R) of the samples with different amount of NdFeB.

electric field to neutralize the impinging EM waves. The phenomenon is called impedance mismatch when parts of EM waves are being reflected and are unable to penetrate the interior of the material [12]. The impedance mismatch is determined by the ratio of impendence of free space (Z_0) to the input impendence (Z_{in}), as Z_0/Z_{in}, Z_0 is approximately equal to 377 Ω. Therefore, with lower input impendence of the material, the ratio gets higher, implying that the EM waves are more likely to reflect. On the contrary, with higher input impendence of the material, the EM waves are more likely to penetrate through the surface of the material, which is beneficial to the absorption of it [43]. The conducting materials obviously have much larger electrical conductivity (σ), which leads to much smaller Z' and Z_{in} as shown in Eq. (7) and Eq. (6), respectively. Therefore, EM waves are in favor of reflection when impinging conducting materials.

The absorption of the EM waves is mainly due to two factors: dielectric loss and magnetic loss. Both of factors are determined by the electronic polarization, the atomic polarization, the orientation polarization, the generation of the internal electric field and the intrinsic magnetic behavior of the material [25,44]. When EM waves enter the material and induce an internal electric-field, the transferring of ions and electrons can be viewed as the energy transfer or loss of the EM waves [45]. When the EM waves interact with the magnetic material, the magnetic moment in the material will align with the magnetic field of the EM waves. Magnetic hysteresis occurs as the direction of the magnetic-field changes, such phenomenon consume the energy of the EM waves to resist the coercivity (H_c) of the magnetic material [25].

Multi-reflection of the EM waves takes place when the EM waves are confined in the material and multiple reflections occurred within the material. The multi-reflection of the EM waves can be ignored if the absorption is higher than 10 dB because multi-reflection is a positive or negative correction term [21].

To study the EMI shielding mechanisms in depth, two samples were prepared, one is 5 wt% MWCNTs sample, the other is 5 wt.% MWCNTs/30 wt.%NdFeB sample. The complex dielectric permittivity ($\varepsilon = \varepsilon' - j\varepsilon''$) and complex magnetic permeability ($\mu = \mu' - j\mu''$) of these two samples are shown in Fig. 7. The measured permittivity and permeability of 5 wt.% MWCNT sample were quite smooth in the employed frequency range. However, the 5 wt.% MWCNT/30 wt.% NdFeB sample possesses some fluctuations to a certain extent. The real (ε', Fig. 7a) and the imaginary (ε'', Fig. 7b) parts of the dielectric permittivity, representing the capability for electrical energy storage and loss, respectively, increase significantly when NdFeB was introduced. Higher permittivity of the composite implies higher electric flux within the composites attributing to the enhanced polarization of electron clouds, which is evidenced by introduction of mixed phases of NdFeB in epoxy composites. The mixed oxidized phases act as scattering centers that disrupt the incoming EM waves.

The real (μ', Fig. 7c) and the imaginary (μ'', Fig. 7d) parts of the magnetic permeability represent the capability for magnetic energy storage and loss, respectively. It is also obvious that the magnetic permeability also increases while NdFeB was added into the composites. When the EM waves impinge on the shielding materials, the intrinsic magnetic moments are arranged along the magnetic field and it changes with time, which generates a hysteresis phenomenon and results in the dissipation of the EM waves. The values of real and imaginary part of magnetic permeability are high comparing with some

Table 4
Comparison of EMI shielding effectiveness of hybrid composites with the literatures.

Composites	Thickness	Content	Transmission Loss (dB)	Reflection Loss (dB)	Ref.
Annealed graphene aerogel/epoxy	4.0 mm	0.8 wt.% GA	30	5	[48]
Graphene nano-sheet/BaTiO3	1.5 mm	4.0 wt.% GNA	42	6	[49]
Sugarcane derived aerogel-like carbon	10.0 mm	–	51	5	[50]
MWCNTs + graphene/PVDF	4.0 mm	2.25 wt.% MWCNTs 2.25 wt.% graphene	45	8	[51]
Acid-modified MWCNTs/polyurethane	1.5 mm	10 wt.% a-MWCNT	29	9	[52]
MWCNTs/ABS	3.0 mm	5 wt.% MWCNT	45	6	[53]
Graphene/PDMS	1.0 mm	0.8 wt.% graphene	20	4	[54]
Graphene/PS	2.5 mm	30 wt.% graphene	29	3	[55]
Nickel-coated carbon fiber/PP	0.5 mm	30 wt.% Ni-CF	48	7	[56]
NdFeB; MWCNTs/epoxy + MWCNT film	1.1 mm	5 wt.% MWCNTs 30 wt.% NdFeB	40	11	This work

reported hard ferrite composite target at microwaves' absorption [26,46,47].

Table 2 shows the comparison of permittivity and permeability between 5 wt.% MWCNTs/30 wt.%NdFeB/Epoxy composites used in this work and the other hard ferromagnetic materials. We can see that the composites fabricated in this study is comparable or even outperform than that of the Barium ferrite which is a hard ferrite usually adopted as EM wave absorbing material recently [26,46,47].

The EMI shielding properties are measured in the frequency range of 8.2–12.4 GHz, known as X band. Fig. 8a and Fig. 8b show the transmission and reflection loss, respectively, of various layers of MWCNT film on the non-woven fabric. Fig. 8c through Fig. 8f show the responses of internal EM waves impinge on the samples, while Fig. 8g and h show the responses of external EM waves impinge on the samples. As we can see in Fig. 8a, the transmission loss increases from around 20 dB to around 40 dB when the layer number increases from one to ten. However, in the meantime, the reflection loss drops from 2 dB to almost none (Fig. 8b). It suggests that with a greater extent of conduction, the MWCNT film leads to the decrement of input impedance, which results in higher Z_0/Z_{in} value and subsequently generates greater impedance mismatch between the MWCNT film and the free space, thus, causes the increase of reflection, leading to the decrease of reflection loss. Fig. 8c and d show the EMI shielding of different weight percentages of MWCNTs with the fixed concentration of NdFeB. All of them seem identical in the transmission loss around 40 dB, but reflection loss increases from 1 dB to 4 dB, which suggested that higher amount of MWCNTs can effectively absorb EM waves within the composite. Fig. 8e and f show the EMI shielding behavior of fixed concentration of MWCNTs with varying concentration of NdFeB. With the increment of NdFeB from 10 wt.% to 30 wt.%, the transmission loss decreases slightly from 40 dB to around 35 dB. However, there exists an obvious distinct peak of 11 dB in reflection loss with 30 wt.% of NdFeB in the sample at 10–11 GHz, which means that over 92% of EM waves are absorbed by the material and less than 8% of EM waves reflect back to the source. In Fig. 8g, we can see that the pattern is similar to that of Fig. 8e, which with the increment of NdFeB, the transmission loss slightly decreases from 40 dB to around 35 dB. However, we can barely obtain much reflection loss as shown in Fig. 8h. Thus, the selective shielding behavior has confirmed.

Comparing with the two situations of the increasing concentration of MWCNTs and the increasing concentration of NdFeB, we can observe that the reflection loss increases more drastically in the latter one. MWCNTs may be efficient to block the EM waves; however, the soaring in electric conductivity may have a negative impact by enlarging the impedance mismatch that leads to the increment of the EM waves' reflection. On the other hand, the electrical conductivity slightly decreases with the increment of the NdFeB, which makes no negative impact to the absorption of the EM waves. In the meanwhile, the mixed oxidized phases of NdFeB can act as scattering centers, which disrupt the impinging EM waves. We can also conclude that this kind of layered structure possesses selective shielding: the sample can reflect almost all of the external EM waves, and absorb most of the internal EM waves. Table 3 list the percentages of transmission, reflection and absorption of different composites composed of different amounts of fillers, which were calculated based on the data obtained between 10 and 11 GHz.

To further investigate the shielding mechanism of the layered structure, the reflection coefficient (R), transmission coefficient (T), absorption coefficient (A) as well as absorption efficiency (A_{eff}) of the layered structure composite were calculated. R and T can be derived directly from the s-parameters listed in the following equations: $R=\left|\frac{E_R}{E_I}\right|^2 = |S_{11}|^2 = |S_{22}|^2$; $T = \left|\frac{E_T}{E_I}\right|^2 = |S_{12}|^2 = |S_{21}|^2$. The absorption coefficient can then be calculated: A = 1 − T − R, and the absorption efficiency was defined as $A_{eff} = \frac{(1-R-T)}{(1-R)}$. Fig. 9 shows the reflection and absorption coefficients of the samples contain same amount of MWCNTs with different amount of NdFeB. As the concentration of the NdFeB increases from 10 wt.% to 30 wt.%, the reflection coefficient decreases from 0.39 to 0.09, in the meanwhile, the absorption coefficient increases from 0.61 to 0.91. These results show that the absorption is the main shielding mechanism of this composite.

The layered composite possesses excellent EMI shielding behavior with absorption dominating mechanism. Also, the fabrication process is very easy and the fabricated composites are very thin in thickness comparing with other works. Table 4 lists some published results focusing on EM wave absorption, and comparisons on the EMI shielding effectiveness in terms of material thickness, transmission loss, as well as reflection loss in the X-band range are made [48–56].

4. Conclusions

The layered composites using MWCNTs/NdFeB/Epoxy as the inner layer and MWCNTs film as the outer layer were designed and fabricated through a very easy route. In the very thin thickness of only around 1.1 mm composites, the inner layer is treated as the absorbent layer that absorbs the EM waves, and the outer layer is treated as reflection layer that rebounds off the EM waves. Different concentrations of NdFeB and MWCNTs have been studied, and the combination of 5%MWCNTs/30% NdFeB/Epoxy layered composites have an optimal absorption efficiency of more than 92% in the range between 10 and 11 GHz, leaving least than 8% of reflection, hence, reduce the possibility of self-disturbance to the device. The reflection coefficient decreases with the increases of NdFeB amount implies that the absorption is the main shielding mechanism of this composites. The selective shielding behavior has also been studied, and it is obvious that the designed structure can effectively reflect over 99.9% of the external EM waves. In the meantime, most of the undesired internal EM waves can be absorbed effectively. According to the design, the devices subjected from internal electromagnetic (EM) wave disturbance and external EM wave interference can be extremely alleviated.

Acknowledgements

The authors thank the support from the Ministry of Science and Technology, Taiwan, under contract number MOST 104-2221-E-007-029-MY3.

Appendix A. Supplementary data

Supplementary data to this article can be found online at https://doi.org/10.1016/j.compositesb.2018.12.130.

References

[1] Baan R, et al. Carcinogenicity of radiofrequency electromagnetic fields. Lancet Oncol 2011;12(7):624–6.
[2] Chung DDL. Carbon materials for structural self-sensing, electromagnetic shielding and thermal interfacing. Carbon 2012;50(9):3342–53.
[3] Shui X, Chung DDL. Nickel filament polymer-matrix composites with low surface impedance and high electromagnetic interference shielding effectiveness. J Electron Mater 1997;26(8):928–34.
[4] Chen Y-J, et al. Investigation of the electric conductivity and the electromagnetic interference shielding efficiency of SWCNTs/GNS/PAni nanocomposites. Diam Relat Mater 2011;20(8):1183–7.
[5] Osawa Z, Kuwabara S. Thermal stability of the shielding effectiveness of composites to electromagnetic interference. Effects of matrix polymers and surface treatment of fillers. Polym Degrad Stabil 1992;35(1):33–43.
[6] Huang CY, Chiou TW. The effect of reprocessing on the EMI shielding effectiveness of conductive fibre reinforced ABS composites. Eur Polym J 1998;34(1):37–43.
[7] Kim BR, et al. Intrinsic electromagnetic radiation shielding/absorbing characteristics of polyaniline-coated transparent thin films. Synth Met 2010;160(17–18):1838–42.
[8] Xiang C, et al. Microwave attenuation of multiwalled carbon nanotube-fused silica composites. Appl Phys Lett 2005;87(12):123103.
[9] Bryning MB, et al. Very low conductivity threshold in bulk isotropic single-walled carbon nanotube-epoxy composites. Adv Mater 2005;17(9):1186–91.
[10] Ameli A, Jung PU, Park CB. Electrical properties and electromagnetic interference

shielding effectiveness of polypropylene/carbon fiber composite foams. Carbon 2013;60:379–91.
[11] Pande S, et al. Improved electromagnetic interference shielding properties of MWCNT-PMMA composites using layered structures. Nanoscale Res Lett 2009;4(4):327–34.
[12] Chen Y, et al. Electromagnetic interference shielding efficiency of polyaniline composites filled with graphene decorated with metallic nanoparticles. Compos Sci Technol 2013;80:80–6.
[13] Li H, et al. Lightweight flexible carbon nanotube/polyaniline films with outstanding EMI shielding properties. J Mater Chem C 2017;5(34):8694–8.
[14] Sharma BK, et al. Synthesis and characterization of polyaniline–ZnO composite and its dielectric behavior. Synth Met 2009;159(5–6):391–5.
[15] Liu Z, et al. Reflection and absorption contributions to the electromagnetic interference shielding of single-walled carbon nanotube/polyurethane composites. Carbon 2007;45(4):821–7.
[16] Liang J, et al. Electromagnetic interference shielding of graphene/epoxy composites. Carbon 2009;47(3):922–5.
[17] Sandler JKW, et al. Ultra-low electrical percolation threshold in carbon-nanotube-epoxy composites. Polymer 2003;44(19):5893–9.
[18] Chen Y-J, et al. Porous composites coated with hybrid nano carbon materials perform excellent electromagnetic interference shielding. Compos B Eng 2015;70:231–7.
[19] Li J, et al. Correlations between percolation threshold, dispersion state, and aspect ratio of carbon nanotubes. Adv Funct Mater 2007;17(16):3207–15.
[20] Jou WS, Cheng HZ, Hsu CF. A carbon nanotube polymer-based composite with high electromagnetic shielding. J Electron Mater 2006;35(3):462–70.
[21] Al-Saleh MH, Sundararaj U. Electromagnetic interference shielding mechanisms of CNT/polymer composites. Carbon 2009;47(7):1738–46.
[22] Li Y, et al. Electrical conductivity and electromagnetic interference shielding characteristics of multiwalled carbon nanotube filled polyacrylate composite films. Appl Surf Sci 2008;254(18):5766–71.
[23] Huang Y, et al. The influence of single-walled carbon nanotube structure on the electromagnetic interference shielding efficiency of its epoxy composites. Carbon 2007;45(8):1614–21.
[24] Kim HM, et al. Electrical conductivity and electromagnetic interference shielding of multiwalled carbon nanotube composites containing Fe catalyst. Appl Phys Lett 2004;84(4):589–91.
[25] Che RC, et al. Microwave absorption enhancement and complex permittivity and permeability of Fe encapsulated within carbon nanotubes. Adv Mater 2004;16(5):401–5.
[26] Verma M, et al. Barium ferrite decorated reduced graphene oxide nanocomposite for effective electromagnetic interference shielding. Phys Chem Chem Phys 2015;17(3):1610–8.
[27] Wang Y, et al. Preparation and electromagnetic properties of Polyaniline(polypyrrole)-BaFe12O19/Ni0.8Zn0.2Fe2O4 ferrite nanocomposites. Appl Surf Sci 2012;259:486–93.
[28] Bhattacharjee Y, Arief I, Bose S. Recent trends in multi-layered architectures towards screening electromagnetic radiation: challenges and perspectives. J Mater Chem C 2017;5(30):7390–403.
[29] Zhao H, et al. Enhanced X-band electromagnetic-interference shielding performance of layer-structured fabric-supported polyaniline/cobalt–nickel coatings. ACS Appl Mater Interfaces 2017;9(38):33059–70.
[30] Biswas S, et al. Absorption-dominated electromagnetic wave suppressor derived from ferrite-doped cross-linked graphene framework and conducting carbon. ACS Appl Mater Interfaces 2017;9(3):3030–9.
[31] Bhattacharjee Y, et al. Construction of a carbon fiber based layer-by-layer (LbL) assembly – a smart approach towards effective EMI shielding. RSC Adv 2016;6(113):112614–9.
[32] Nam IW, Lee HK, Jang JH. Electromagnetic interference shielding/absorbing characteristics of CNT-embedded epoxy composites. Compos Appl Sci Manuf 2011;42(9):1110–8.
[33] Rao AM, et al. Diameter-selective Raman scattering from vibrational modes in carbon nanotubes. Science 1997;275(5297):187–91.
[34] Fang J, et al. A wormhole-like porous carbon/magnetic particles composite as an efficient broadband electromagnetic wave absorber. Nanoscale 2016;8(16):8899–909.
[35] Zhang N, Huang Y, Wang M. 3D ferromagnetic graphene nanocomposites with ZnO nanorods and Fe_3O_4 nanoparticles co-decorated for efficient electromagnetic wave absorption. Compos B Eng 2018;136:135–42.
[36] Nunesa RAX, et al. Wear, friction, and microhardness of a thermal sprayed PET - poly (ethylene terephthalate) coating. Mater Res 2009;12(2):121–5.
[37] Xu J, et al. Simultaneous adsorption and dechlorination of 2,4-dichlorophenol by Pd/Fe nanoparticles with multi-walled carbon nanotube support. J Hazard Mater 2012;225–226:36–45.
[38] Wei H, et al. Synthesis of ferromagnetic Nd2Fe14B nanocrystalline via solvothermal decomposition and reduction–diffusion calcination. IEEE Trans Magn 2015;51(11):1–4.
[39] Xu H, Hu XL, Zhang LZ. Generalized low-temperature synthesis of nanocrystalline rare-earth orthoferrites $LnFeO_3$ (Ln = La, Pr, Nd, Sm, Eu, Gd). Cryst Growth Des 2008;8(7):2061–5.
[40] Mir SA, Ikram M, Asokan K. Structural, optical and dielectric properties of Ni substituted NdFeO3. Optik - Int J Light Electron Opt 2014;125(23):6903–8.
[41] Rhim SM, et al. Effects of B_2O_3 Addition on the dielectric and ferroelectric properties of $Ba_{0.7}Sr_{0.3}TiO_3$ ceramics. J Am Ceram Soc 2000;83(5):1145–8.
[42] Vinoy KJ, Jha RM. Radar absorbing materials : from theory to design and characterization. Boston: Kluwer Academic Publishers; 1996.
[43] Song W-L, et al. Flexible graphene/polymer composite films in sandwich structures for effective electromagnetic interference shielding. Carbon 2014;66:67–76.
[44] Chen T, et al. Hexagonal and cubic Ni nanocrystals grown on graphene: phase-controlled synthesis, characterization and their enhanced microwave absorption properties. J Mater Chem 2012;22(30):15190.
[45] Ott HW. Electromagnetic compatibility engineering. Hoboken, United States: John Wiley & Sons Inc; 2009.
[46] Verma V, Kapil J, Singh N. Structural, magnetic properties of soft and hard ferrites and their EMI shielding application in X-band frequency range. Int J Eng Res Technol 2014;3(12).
[47] Durmus Z, Durmus A, Kavas H. Synthesis and characterization of structural and magnetic properties of graphene/hard ferrite nanocomposites as microwave-absorbing material. J Mater Sci 2014;50(3):1201–13.
[48] Li XH, et al. Thermally annealed anisotropic graphene aerogels and their electrically conductive epoxy composites with excellent electromagnetic interference shielding efficiencies. ACS Appl Mater Interfaces 2016;8(48):33230–9.
[49] Yuchang Q, et al. Graphene nanosheets/BaTiO3 ceramics as highly efficient electromagnetic interference shielding materials in the X-band. J Mater Chem C 2016;4(2):371–5.
[50] Li Y-Q, et al. Lightweight and highly conductive aerogel-like carbon from sugarcane with superior mechanical and EMI shielding properties. ACS Sustainable Chem Eng 2015;3(7):1419–27.
[51] Ma X, et al. Porous superhydrophobic polymer/carbon composites for lightweight and self-cleaning EMI shielding application. Compos Sci Technol 2018;158:86–93.
[52] Gupta TK, et al. Improved nanoindentation and microwave shielding properties of modified MWCNT reinforced polyurethane composites. J Mater Chem 2013;1(32):9138.
[53] Schmitz DP, et al. Hybrid composites of ABS with carbonaceous fillers for electromagnetic shielding applications. J Appl Polym Sci 2018;135(29):46546.
[54] Chen Z, et al. Lightweight and flexible graphene foam composites for high-performance electromagnetic interference shielding. Adv Mater 2013;25(9):1296–300.
[55] Yan D-X, et al. Efficient electromagnetic interference shielding of lightweight graphene/polystyrene composite. J Mater Chem 2012;22(36):18772–4.
[56] Lee SH, et al. Effects of processing methods on the electrical conductivity, electromagnetic parameters, and EMI shielding effectiveness of polypropylene/nickel-coated carbon fiber composites. Macromol Res 2017;25(9):936–43.